The Canadian Mineralogist
Vol. 57, pp. 1-21 (2019)
DOI: 10.3749/canmin.1800074

MINERALOGY AND WEATHERING OF REALGAR-RICH TAILINGS AT A FORMER As-Sb-Cr MINE AT LOJANE, NORTH MACEDONIA

TAMARA ĐORĐEVIĆ[§]

Institut für Mineralogie und Kristallographie, Universität Wien, Althanstr. 14, 1090 Wien, Austria

UWE KOLITSCH

Mineralogisch-Petrographische Abteilung, Naturhistorisches Museum, Burgring 7, 1010 Wien, Austria
Institut für Mineralogie und Kristallographie, Universität Wien, Althanstr. 14, 1090 Wien, Austria

TODOR SERAFIMOVSKI AND GORAN TASEV

Department of Mineral Deposits, Faculty of Natural and Technical Sciences, University "Goce Delčev"-Štip, Goce Delčev 89, 2000 Štip, North Macedonia

NATHALIE TEPE

Department of Environmental Geosciences, University of Vienna, Althanstr. 14, 1090 Wien, Austria

MICHAEL STÖGER-POLLACH

University Service Centre for TEM, Technische Universität Wien, Wiedner Hauptstr. 8-10, 1040 Wien, Austria

THILO HOFMANN

Department of Environmental Geosciences, University of Vienna, Althanstr. 14, 1090 Wien, Austria

BLAŽO BOEV

Department of Mineral Deposits, Faculty of Natural and Technical Sciences, University "Goce Delčev"-Štip, Goce Delčev 89, 2000 Štip, North Macedonia

ABSTRACT

In the Lojane area (North Macedonia) ores of Sb (stibnite), As (realgar), and Cr (chromite) were mined and processed in a metallurgical plant until 1979. Over one million tons of flotation tailings containing As, Sb, and other hazardous substances are located in an open dump site for flotation waste created by the mine. The tailings site is completely unprotected, and its orange color reflects a very high concentration of arsenic (fine-grained realgar superficially altered to pararealgar). In order to better understand the weathering behavior of these tailings, which is necessary to evaluate the environmental risks (mainly from the mobilization of As-Sb-Cr), solid waste material was sampled and studied from the chemical and mineralogical point of view. The material was characterized by inductively coupled plasma-mass spectrometry (ICP-MS), inductively coupled plasma-optical emission spectrometry (ICP-OES), X-ray diffraction analysis (both single crystal and powder), scanning electron microscopy (SEM) with energy-dispersive microanalysis (EDX), Raman spectroscopy, and transmission electron microscopy (TEM) with selected area electron diffraction (SAED), energy-dispersive X-ray analysis (EDX), and electron energy loss spectrometry (EELS). The studied tailings material is comprised mostly of well-crystallized realgar, gypsum, and quartz, and minor amounts of stibnite, pararealgar, chromite, and sulfur. Very minor pyrite is found within quartz aggregates. The most abundant secondary phase, which forms thin coatings around realgar and stibnite grains, is an As-Sb-Fe-Ca-(Ni)-oxide/hydroxide in which the As:Sb ratio varies from *ca*. 2:1 to 1:2.2 and Fe contents are variable. Antimony-dominant variants of

[§] *Corresponding author e-mail address*: tamara.djordjevic@univie.ac.at

this oxide also form larger homogeneous grains up to 500 μm in size, characterized by broad dehydration cracks suggesting original formation as a gel. Both As-rich and -poor variants were identified as members of the roméite group. EELS showed that all the Fe is ferric. Further secondary phases originated from the weathering of realgar, stibnite, and other primary phases are As-bearing sulfur, scorodite (often slightly Sb-bearing, locally common), arsenolite, "limonite", pickeringite (Ni- and Fe-bearing), alunogen, and annabergite. The weathering of primary sulfides in the flotation tailings at Lojane proceeded under mostly oxidizing, acidic, and temporarily wet conditions. Highly acidic conditions on the surface of the tailings dump imply dissolution of arsenolite and scorodite, thus causing contamination of the environment and high mobility of arsenic.

Keywords: arsenic, realgar, antimony, tailings, oxidation, weathering.

Introduction

Arsenic (As) has been classified as one of the major pollutants by the United States Environmental Protection Agency (USEPA 2009), contested in its toxicity by only a few other elements. Like As, antimony (Sb) is classified as a priority pollutant by the same Agency and has been assigned to the group of substances suspected of being carcinogenic to humans by the International Agency for Research on Cancer.

One of the major sources of As and Sb in the environment is mine wastes, which contain tens to tens of thousands of ppm of arsenic and tens to thousands of ppm of antimony (Kossoff *et al*. 2015 and references therein). Most of the environmental risks concerning mine wastes are due to the constant element release from mechanically unstable, chemically labile, and non-remediated mine tailings and from abandoned former mine sites where waste materials are subjected to atmospheric conditions, underground or meteoric waters, or biotic effects (organisms living on the site or nearby). These alteration processes lead to contamination of the environment in addition to a general background level of contamination (Hudson-Edwards 2016).

One of the ways to reduce the risk posed by exposure to As and Sb is the precipitation of secondary minerals, especially those that are less soluble and have low bioavailability. Through both weathering and alteration by ore processing of primary As and Sb minerals, secondary oxides and oxysalts of As and Sb are formed. Native As, As-bearing sulfides (arsenopyrite, As-bearing pyrite, realgar, orpiment), and As-bearing sulfosalts (*e.g*., enargite, tennantite) are the most widespread primary arsenic minerals in mining-affected environments. Weathering of these arsenic minerals generally releases arsenic into the environment and thus potentially causes significant contamination. The released As can precipitate as various secondary arsenic minerals that contain structural arsenic. These comprise Fe arsenates such as scorodite and kaňkite, Fe sulfoarsenites such as tooeleite, Ca-Fe arsenates such as arseniosiderite, yukonite, and related amorphous forms, and Ca(-Mg) arsenates such as pharmacolite and picropharmacolite (Drahota & Filippi 2009, Majzlan *et al*. 2014). These precipitation processes cause the sequestration of active arsenic species, significantly reducing the arsenic toxicity in the environment. Arsenic can also be incorporated in trace amounts in a variety of minerals such as Fe, Mn, or Al oxides, Fe, Mn or Al hydroxides, Fe, Mn, Al sulfates, other hydrous and anhydrous sulfates, phosphates, and hydrous silicates (Majzlan *et al*. 2011). In these cases, the arsenic is taken up by sorption onto the mineral surface (Mohan & Pittman 2007) or incorporated into the mineral structure by co-precipitation. The importance of such processes in modifying arsenic bioavailability indicates a continued need to investigate secondary As-bearing minerals and related phase transformations that occur in sulfide mine environments, in order to improve our understanding of the environmental geochemistry of As.

Antimony is mined mostly from hydrothermal ores that are usually dominated by stibnite. Other primary Sb sulfides and rare sulfosalts may be present in smaller amounts (Roper *et al*. 2012). In hydrothermal ores, antimony may be present in appreciable amounts even if it is not targeted as the element of interest (*e.g*., in tetrahedrite) and, therefore, will be included in ore processing and disposal of waste. If exposed to the ambient atmosphere, the primary Sb sulfides give way to a limited number of Sb-bearing secondary minerals (Roper *et al*. 2012). In tailings impoundments, the primary or secondary minerals can be converted to tertiary minerals typical for these settings. The environmental mobility of Sb has been evaluated using various sequential leaching protocols or dissolution studies (Ashley *et al*. 2003, Flynn *et al*. 2003 and references therein). These authors concluded that the oxidation of stibnite is rapid. The products of this oxidation are the Sb oxide minerals senarmontite, valentinite, stibiconite, or rarely cervantite. The solubility of these minerals is variable; in a sufficient water flow, they may slowly release Sb into the environment. However, at most of these sites, secondary Fe oxides form a formidable barrier to Sb mobility (Ashley *et al*. 2003, Majzlan *et al*. 2007). Therefore, as long as these Fe oxides are not disturbed,

Sb may not be bioavailable (Flynn *et al*. 2003), although there seem to be some exceptions (Burton *et al*. 2019).

Large amounts of mining and processing waste were generated at the Lojane site (Sb–As–Cr deposit) in northeast North Macedonia during the second half of the last century and the remediation of this site has not proceeded despite United Nations Environment Programme (UNEP) and United Nations Development Programme (UNDP) initiatives in the mid-2000s (UNEP 2000, JICA *et al*. 2008, Williams & Marstijepović 2010). Since the mineralogical composition of mining wastes is the key factor that controls retention and release of pollutants, the major aim of this study was the characterization of the crystalline primary and secondary minerals of the mine-waste materials and of the amorphous and poorly crystalline secondary mineral phases.

The literature on the mineralogical composition of the Lojane deposit is fairly poor, consisting mostly of a very few scientific articles and conference reports from the 1930s to the 1960s, some only in Serbian or Macedonian (Hiessleitner 1931, 1934, 1951, Radusinović 1956, 1966, Janković 1960, Antonović 1965, and references therein). To our knowledge, the weathering products of the primary minerals as well as the mineralogy of the various mine waste materials have not been studied.

We have started to study the environmental mineralogy and geochemistry of the Lojane Sb-As-Cr deposit in detail in a four-year project (1/2018–12/2021), which was preceded by a smaller mobility support bilateral research project between Austria and Macedonia (07/2016–06/2018) that aimed to characterize weathering products in various dumps of the Lojane deposit. A first study focusing on the mineralogy of secondary phases detected on weathered ore-bearing waste dumps (*i.e*., excluding the flotation waste) has been published by our group (Kolitsch *et al*. 2018).

The present study focuses only on how As, Sb, and other toxic elements are hosted in the oxidation products of the realgar-rich flotation tailings. Using freshly collected samples from these tailings, which contain very abundant realgar and pararealgar (on average 60 wt.%), as well as notable amounts of stibnite (between 5.9 and 13.45 wt.% stibnite), we have characterized pre-weathering phases and weathering products using inductively coupled plasma-mass spectrometry (ICP-MS), inductively coupled plasma-optical emission spectrometry (ICP-OES), X-ray diffraction analysis (both single crystal and powder), scanning electron microscopy (SEM) with energy-dispersive microanalysis (EDX), Raman spectroscopy, and transmission electron microscopy (TEM) with selected area electron diffraction (SAED), energy-dispersive X-ray (EDX), and electron energy loss spectroscopy (EELS). We use these results to discuss the natural oxidation of realgar and stibnite and associated implications for the transformation and mobility of As and Sb.

Site Description and Geology

Site description

The abandoned Sb-As-Cr deposit Lojane in northeast North Macedonia is located near the border with Serbia and Kosovo, between the villages of Lojane and Vaksince (Fig. 1). The mine presents a major environmental problem for North Macedonia. The site is located near two villages and a local school. It presents a very serious human health risk, given the high concentration of arsenic wastes (Alderton *et al*. 2014 and references therein).

The mine exploited and processed As-, Sb-, and Cr-ores in the period between 1923 and 1979. Over one million tons of tailings containing As, Sb, and other hazardous substances are located in an open dump site for flotation waste created by the mine (Fig. 2a). The production and beneficiation facilities, ore waste dumps, and tailings ponds were abandoned without carrying out any conservation or protective measures. The waste material is estimated to comprise 20,000 t at the mine site and 15,000 t of arsenic concentrate and 3,000,000 t of tailings at the concentration facility (Antonović 1965). The tailings dump (42.217303 N, 21.664378 E) is completely unprotected and its orange color suggests a very high concentration of realgar and its weathering products (Alderton *et al*. 2014). The concentrate was transported by small gauge railway to a location next to the main railway line at Čivluk. There are also the remains of the old arsenic smelter (Fig. 3). The smelter site contains a large pile of arsenic concentrate and is covered with numerous heaps of black and white powder. These consist of stibnite concentrate and refined arsenolite and are assumed to be the remains of 2500 wooden barrels of processed material, which were abandoned and left to rot.

The potential environmental risk includes elevated concentrations of As and Sb leaching out of flotation tailings into the surrounding soils, ground, and surface waters (Tasev *et al*. 2017). The pH values of ground waters near the studied flotation tailings are around 8 (Alderton *et al*. 2014). The soils in the immediate vicinity of the flotation tailings exhibit very high concentrations of As, Sb, and Ni. Furthermore, Janković (1989) reported an increased Tl content in the realgar from Lojane (100–1000 ppm). The tailings material is exposed to the weather, resulting in continued physical transport *via* rivers and wind-

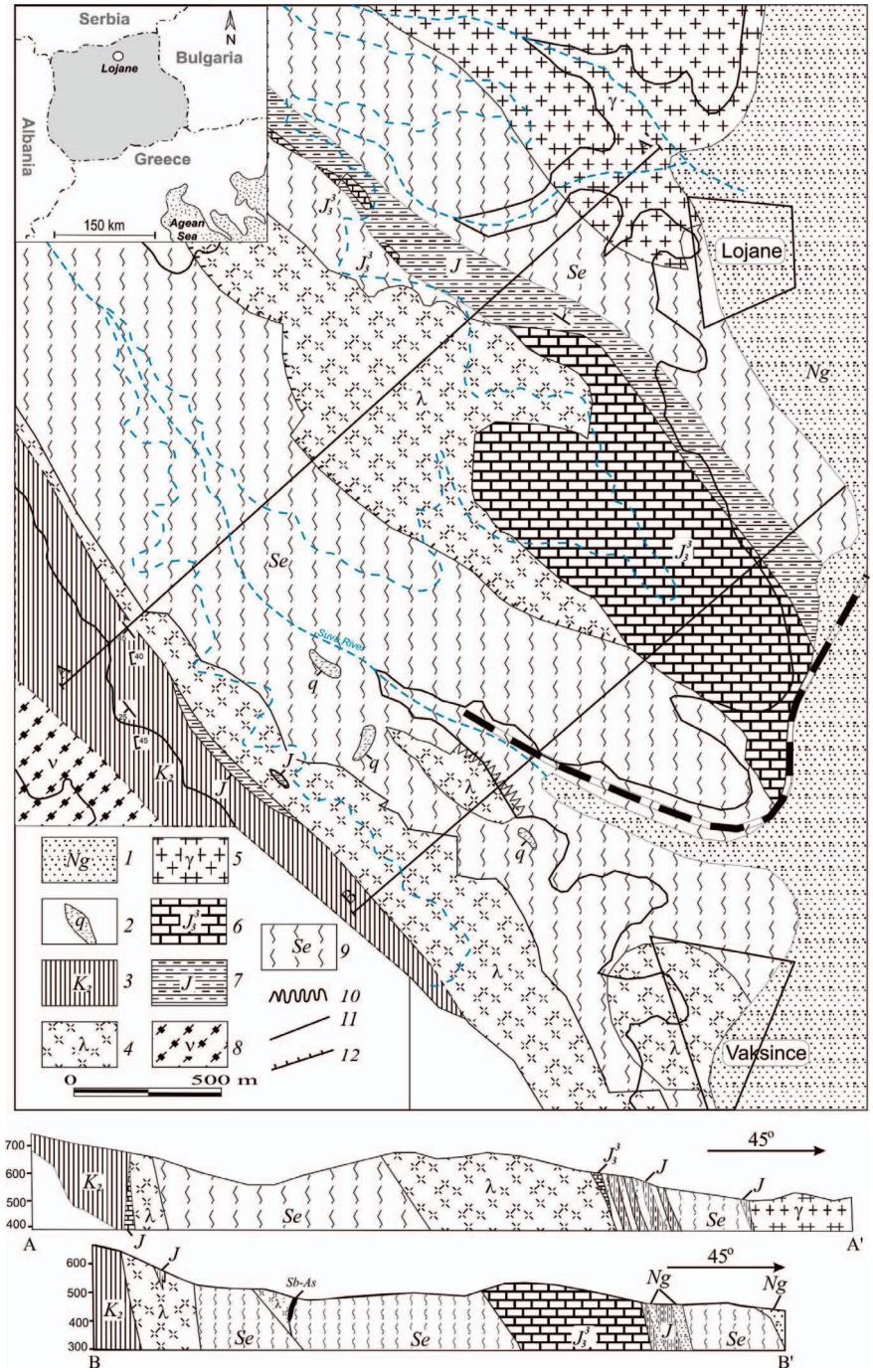

FIG. 1. Geological map of the Lojane deposit area (Tasev *et al*. 2017, adapted from Antonović 1965): (1) diluvial and Neogene deposits; (2) silicified serpentine; (3) Upper Cretaceous flysch; (4) quartz-porphyry (rhyolite); (5) granite, syenite; (6) Upper Jurassic massive limestone; (7) black shale, sandstone (diabase-hornfels formation, Jurassic); (8) gabbro, diorite; (9) serpentinite and peridotite; (10) realgar (As) and stibnite (Sb) mineralization; (11) normal fault; (12) reverse fault.

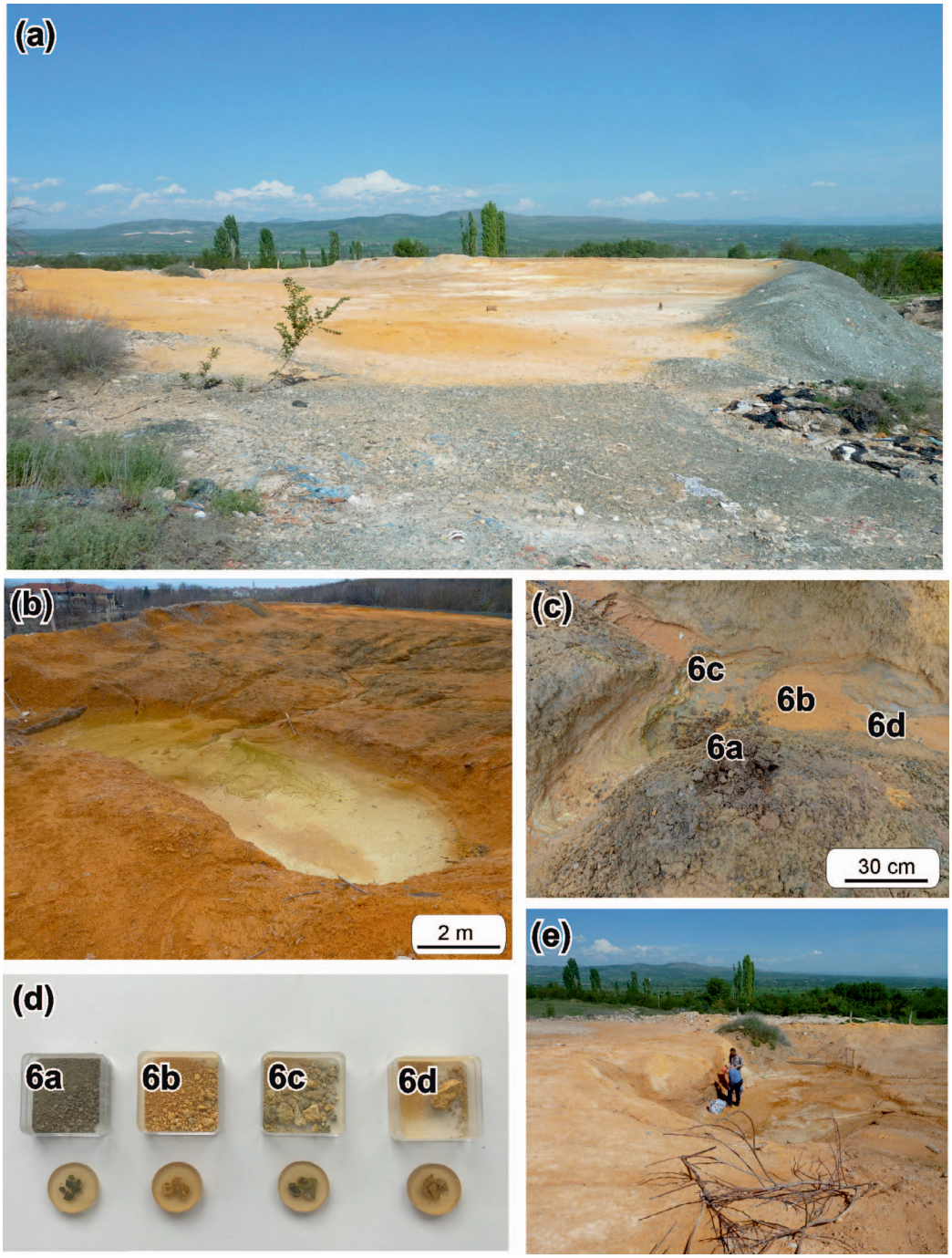

FIG. 2. Information about samples: (a) open dump site for flotation waste; (b) ellipsoid-shaped hole, from which samples 6a–6d were taken; (c) sampling points; (d) part of the sample material and their resin-mounted polished sections; and (e) sampling profiles.

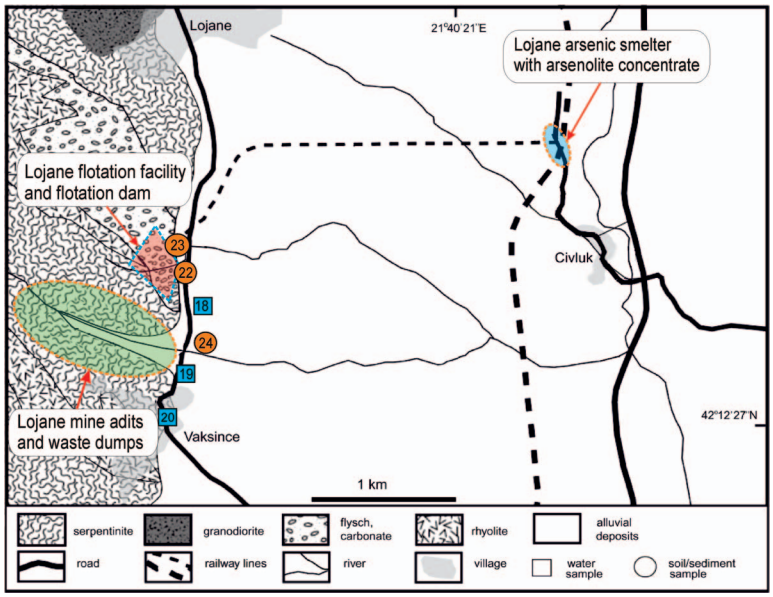

FIG. 3. Topographic map of the Lojane area with locations of the zones of interest. Sampling points for water are marked as blue squares and those for soil and sediment samples as light orange circles.

blown dust, as well as chemical weathering and transport in solution, which increases the environmental impact. The climate in the Lojane area (altitude: about 440 to 640 m) is mild and generally warm; the average annual temperature is 11.2 °C and the average rainfall is 544 mm per year.

Geological setting and ore-deposit mineralogy

In the wider area of the Lojane deposit, several characteristic types of rocks have been identified, among which a serpentinite (ophiolite) and a rhyolite of Tertiary age dominate. The geological setting also comprises young granite (with numerous apophyses), Jurassic limestone, black tuff-like sandy claystone, flysch sediments, and Neogene sediments (extensive alluvial gravels to the east). The Cr deposit consists of several chromite lenses and layers hosted by the serpentinite. The vein- to stockwork-like hydrothermal As-Sb (realgar and stibnite) mineralization, which is a result of the intrusion of a rhyolite body, mainly consists of steeply dipping, NW–SE trending veins (maximum thickness 3–4 m, on average 1–2 m). It extends along the contact between the rhyolite and the older, strongly silicified serpentinite, and also into the serpentinite and its chromite ores to a distance of about 0.5 km. In addition, in the northwestern part there are insignificant stibnite occurrences, some with traces of realgar in two masses of silicified serpentinite, 100 and 400 m from the end of the rhyolite lens (Fig. 1). The Sb-As ore is very unevenly distributed in the mineralized area, such that in the area of contact with the rhyolite in the southeastern part of the deposit only 50% of the ore is located at a level of 480 m, while the other half is in the deeper levels in the serpentinite.

After the first geological mapping studies of the area (Hiessleitner 1931, 1934, 1951, see also Schumacher 1954), which focused on the chromite deposit, fairly detailed descriptions of both geology and As-Sb ore mineralization were given by Janković (1960) and Radusinović (1966). A comprehensive study of the geology, tectonic structure, and genesis of the As-Sb deposit was provided by Antonović (1965). He observed ore textures reflecting the low-temperature and tectonized character of the mineralization (*e.g.*, dolomite veins with realgar, chalcedony gangue, breccias, microbreccias, collomorphic ore types, spherulitic stibnite, and stibnite replaced by realgar). The only subsequent studies are those of Grafenauer (1977), who focused on the chromite deposit, and Augé *et al.* (2017), who reported on some platinum-group minerals detected in the ophiolite-hosted chromite ore.

It should be emphasized that the rhyolites were defined differently by different authors. Namely, they have been described as porphyries (Gripp 1922), as andesite (Hiessleitner 1934, 1951, Serafimovski 1993), and as dacite (Tućan 1936), while according to Divljan (1957) these rocks are mainly rhyolites; only small

intruded bodies within the Lojane granites were defined as dacite.

The main ore minerals observed by Janković (1960) and Antonović (1965) were sulfides of As and Sb (realgar, stibnite, rare orpiment), but Ni-bearing pyrite [(Fe,Ni,Co)S_2], vaesite (NiS_2), cattierite (CoS_2), kermesite (Sb_2S_2O), pyrite, marcasite, molybdenite, and "pitchblende" (uraninite) were also reported to occur in minor quantities. The gangue consists of fine-grained quartz and minor dolomite. As shown by our re-study of the Lojane deposit, which started in 2016, some oxidation of the primary ore phases has resulted in the formation of secondary oxides, hydroxides, sulfates, and arsenates. Our latest findings by SEM-EDX, EPMA, Raman spectroscopy, and single-crystal and powder XRD (Đorđević *et al*. 2017, 2018, Kolitsch *et al*. 2018) proved the presence of (in alphabetical order) the following minerals: albite, alunogen, annabergite, aragonite, arsenic, baryte, chalcopyrite, coffinite, duranusite, epidote, eulytine, fluorapatite, galena, gersdorffite (previously overlooked, but fairly common according to our results), hercynite, hexahydrite, hörnesite (the predominant secondary arsenate on weathered ore specimens), hydromagnesite, hydroxylapatite, kaňkite, kaolinite-group representatives, laurite, "limonite", magnesite, magnesiochromite, magnetite, maucherite(?), millerite, monazite-(Ce), muscovite to illite, naldrettite(?), parkerite(?), pentlandite, pickeringite, polydymite(?), pyrrhotite, roméite-group minerals, rozenite, rutile, scorodite, senarmontite, spinel, stibiconite, As-bearing sulfur, tripuhyite(?), As-rich ullmannite, uvarovite, valentinite, violarite, and an unnamed Bi-As-S-Cl(-O?) phase. Investigations of the complex primary mineralogy of both realgar-stibnite and chromite ore mineralizations are ongoing.

Materials and Methods

The preliminary sampling and documentation of the realgar-rich flotation tailings (Fig. 2a) were undertaken for the first time in November 2016 (cold and rainy period). Four samples weighing *ca*. 500–600 g each (labeled 6a–6d) were taken from the subsurface (to a depth of 10 cm at which point the samples were already very wet) from an ellipsoid-shaped hole (*ca*. 2 × 3 m in area, depth approx. 1.5–1.7 m) in the northern end of the flotation dump, where the runoff water collects (Fig. 2b). These representative samples, studied in detail (see below), differ clearly from each other with respect to their color, consistency (depending on the number of secondary phases cementing individual grains and aggregates), porosity, and bulk morphology (Fig. 2c and d). The wetter and the darker the tailings, the more reduced conditions are assumed to have been during the sampling time.

Further samples along the profile (Fig. 2e) were collected in May 2017 (dry period) and were analyzed using powder X-ray diffraction and partly by Raman spectroscopy. However, these additional samples did not show any notable differences (by comparison to the above four samples) in chemical and mineralogical compositions, except for the presence of arsenolite (PXRD, Raman) as well as alunogen and Ni- and Fe-bearing pickeringite (Raman, EDX) in the surface part of the profile.

Some minerals were separated with a binocular microscope and identified by single X-ray diffraction (SXRD) using a Nonius KappaCCD four-circle single-crystal diffractometer (Mo tube, graphite monochromator, CCD area detector), equipped with a 300 μm diameter capillary-optics collimator (Institut für Mineralogie und Kristallographie, University of Vienna).

The samples selected for powder X-ray diffraction (PXRD) were homogenized and powdered by fine grinding in an agate mortar. Homogeneous powders of all four samples were analyzed with a Bruker D8 Advance diffractometer (θ-θ type with scintillation counter) under the following conditions (Institut für Mineralogie und Kristallographie, University of Vienna): Cu$K\alpha$ radiation, position-sensitive Lynxeye detector, 40 kV, 25 mA, step scanning in the angular range of 5° to 85° 2θ at room temperature. The step size was set to 0.01° 2θ and dwell time to 1 s per step. DIFFRAC.EVA software, version 4.2, and the ICDD powder diffraction file PDF-2 were used for peak and phase identification. Using the program *TOPAS* (Bruker 2017), we refined the fractions of the individual minerals by the Rietveld method (supplementary material[1], Fig. Sl).

Raman spectra of the polished sections (embedded in resin) were measured with a Horiba LabRam-HR system equipped with an Olympus BX41 optical microscope in the spectral range between 100 and 4000 cm^{-1} (Institut für Mineralogie und Kristallographie, University of Vienna). The 632.8 nm excitation line of a He–Ne laser was focused with a 50× or 100× objective (N.A. = 0.90) on the randomly oriented crystals and aggregates. The spectra were acquired with a nominal exposure between 10 and 60 s (confocal mode, 1800 lines/mm, 1.5 μm lateral resolution, and approximately 3 μm depth resolution). The density of the laser power was adjusted depending

[1] Supplementary Data are available from the Depository of Unpublished data on the MAC website (http://mineralogicalassociation.ca/), document "Realgar-rich tailings, CM57, 1800074".

on the mineral measured and to avoid possible sample changes due to intense laser-light absorption and resulting temperature increase.

Chemical compositions and micromorphologies of mineral phases were studied using carbon-coated polished samples or loose crystals and crystal aggregates with a JEOL JSM-6610 LV scanning electron microscope (SEM) with a W filament (15 kV), equipped with an energy-dispersive X-ray (EDX) detector (Bruker e-FlashHR+, resolution 127 eV) and Bruker Esprit 2.0 software (Natural History Museum, Vienna).

Chemical information was obtained by employing electron energy loss spectrometry (EELS) coupled with transmission electron microscopy (TEM). For this purpose, a FEI TECNAI F20 instrument, which is equipped with a GATAN GIF Tridiem energy filter and an EDAX APOLLO XII EDX detector, was used. Data treatment was done using DigitalMicrograph™ software. The EELS measurements were conducted in scanning mode with a spatial resolution of 0.7 nm. Quantitative chemical analysis using EELS and/or EDX has 10% relative error due to spectral noise. SAED was performed by inserting a 120 nm aperture in the image plane of the objective lens and parallel illumination conditions.

Major and trace element concentrations in the four selected tailings samples were determined by quadrupole ICP-MS (Agilent 7900) and ICP-OES (Perkin Elmer Optima 5300 DV) in the Department of Environmental Geosciences at the University of Vienna. The milled and homogenized samples were pressure-digested at 225 °C in a mixture of 3 mL of 30% suprapure hydrochloric acid (HCl), 1 mL of 65% suprapure nitric acid (HNO_3), and 1 mL of 40% suprapure hydrofluoric acid (HF) in polytetrafluoroethylene (PTFE) vessels using a Pico Trace DAS acid digestion system, following the protocols of Alexander (2008) and Dulski (2001). When the decomposition of the samples was complete, all acid mixtures were evaporated to incipient dryness and redissolved in 5 mL of 65% suprapure HNO_3. This step was repeated twice before the samples were taken up in 2% suprapure HNO_3 and analyzed by ICP-MS and ICP-OES. To ensure data quality the certified reference material IF-G was also pressure-digested and analyzed for major and trace elements.

Groundwater and soil materials were sampled in 2012 as part of the "NATO-Science for Peace" project involving two of the co-authors from North Macedonia (GT and TS). These samples were taken from the immediate vicinity of the villages of Lojane and Vaksince. Details of sampling and laboratory measurements are given in Alderton *et al*. (2014). Measured concentrations of As and Sb in soils and waters were compared to various national reference guidelines to assess their significance. There is some variation in the values for these guidelines and the data for Sb are not as comprehensive as those for As (Alderton *et al*. 2014, Tasev *et al*. 2017). This is because the values may be set for local conditions, but also because they have been derived using different ecotoxicological tests or for different applications (*e.g*., drinking water, irrigation, environmental well-being, intervention).

Chemical Composition of the Tailings

Major and trace element concentrations of the mine tailings are shown in Table 1. The rare earth element concentrations are given in the supplementary material (Table S1). The analyzed samples show very high concentrations of Cr, Ni, As, and Sb. In particular, arsenic concentrations range from 223 to 345 g/kg (median 268 g/kg As) and antimony concentrations range from 80.8 to 114 g/kg (median 98 g/kg Sb). Furthermore, the concentrations range from 632 to 796 mg/kg for Cr (median 737 mg/kg Cr) and from 103 to 5640 mg/kg for Ni (median 1884 mg/kg Ni). Samples 6a (5640 mg/kg Ni) and 6c (3628 mg/kg Ni) show remarkably higher Ni concentrations compared to samples 6b (140 mg/kg Ni) and 6d (103 mg/kg Ni). Thallium was not detected, casting some doubt on the results of Janković (1989).

Random 'grab' samples from the piles of abandoned concentrate material at the Lojane smelter site were previously sampled by Alderton *et al*. (2014). The locations of their soil samples 22 and 23 are close to those for our tailings samples 6a to 6d. While soil samples 22 and 23 from Alderton *et al*. (2014) showed higher concentrations of CaO, Fe_2O_3, MgO, and MnO, the tailings samples show remarkably higher concentrations for Ti, As, and Sb, indicating a stronger environmental impact factor.

Chemical composition of the groundwater

The groundwater samples collected from the immediate vicinity of the flotation tailings (samples 18, 19, 20; see Fig. 3) showed an alkaline character, pH from 8.0 to 8.3 (Alderton *et al*. 2014), and elevated electric conductivities (>700 μS/cm). This is in accordance with the dominant lithology, mainly serpentinite (containing abundant Mg silicates; Hiessleitner 1934, 1951, Schumacher 1954, Tasev *et al*. 2017) as well as dolomite/limestone (Alderton *et al*. 2014).

In the sampled groundwaters, directly or intermediately influenced by the presence of mineralization, waste dump, and flotation tailings, the concentrations of arsenic ranged from 54.6 to 402 mg/kg As (median

TABLE 1. MAJOR AND TRACE ELEMENT CONCENTRATIONS OF TAILINGS SAMPLES 6a TO 6d AND THE CERTIFIED REFERENCE MATERIAL IF-G*

		Chemical composition of the tailings samples						
	Unit	6a	6b	6c	6d	CRM IFG	LLoD**	Unit
Al_2O_3	wt.%	2.50	1.09	2.92	1.02	0.13	50	µg/kg
CaO	wt.%	6.19	4.84	5.30	0.71	1.66	50	µg/kg
Fe_2O_3	wt.%	3.81	3.68	3.55	2.46	57.9	50	µg/kg
K_2O	wt.%	0.55	0.12	0.37	0.12	0.018	20	µg/kg
MgO	wt.%	1.98	0.21	1.77	0.34	2.02	20	µg/kg
MnO	wt.%	0.067	0.001	0.050	0.002	0.042	5	µg/kg
Na_2O	wt.%	0.11	0.022	0.088	0.027	0.014	20	µg/kg
Li	mg/kg	12.7	7.16	23.8	6.01	0.144	15.3	µg/kg
P	mg/kg	172	347	89.2	49.6	70.2	5	µg/kg
Sc	mg/kg	2.30	1.74	3.98	1.54	0.205	12.2	µg/kg
Ti	mg/kg	461	294	491	303	21.2	5	µg/kg
Cr	mg/kg	792	632	796	682	<LLoD	10	µg/kg
Ni	mg/kg	5640	140	3628	103	23.6	5	µg/kg
As	g/kg	232	303	223	345	<LLoD	10	µg/kg
Sb	g/kg	114	80.8	89.7	105	<LLod	10	µg/kg
Co	mg/kg	176	6.67	186	4.07	3.32	1.04	µg/kg
Rb	mg/kg	24.2	9.29	25.4	8.18	0.284	2.74	µg/kg
Sr	mg/kg	78.0	22.8	65.4	8.29	3.43	6.32	µg/kg
Cs	mg/kg	12.0	22.7	24.1	22.6	0.059	0.339	µg/kg
W	mg/kg	25.8	34.6	61.8	34.3	0.57	10.2	µg/kg
Pb	mg/kg	23.5	22.7	28.9	18.6	5.42	3.85	µg/kg
Th	mg/kg	1.08	0.79	2.06	0.54	0.054	1.36	µg/kg
U	mg/kg	19.3	36.6	38.5	22.9	0.017	0.320	µg/kg

* Values for the REE are given in the supplementary material (Table S1).
** The lower limit of detection (<LLoD) values are based on (3 × SD + average value of the Picotrace blank) of the respective element.

175.7 mg/kg As), while the values for antimony ranged from 5.7 to 166.3 mg/kg Sb (median 60 mg/kg Sb). For all samples there is a close positive correlation between As and Sb (correlation coefficient 0.999). There appears to be no major variation in concentration of either As or Sb with pH (Alderton *et al*. 2014). In all of the water samples As concentrations exceed the 10 µg/L value accepted for safe drinking water (UK standard) and the stricter 5 µg/L MDK value (North Macedonian standard). Contrary to that, two of three Sb concentrations are lower than 10 µg/L and are within the acceptable limits for this element. Waters sampled from position 19 (from Vaksince in particular) showed contents of As and Sb that are well above the drinking water limits set by the various regulatory agencies. Here we would like to stress that, besides the anthropogenic influences of the former mining activities, increased concentrations of As are also the result of a high natural local geochemical background of this element, and all wells drilled in serpentine are naturally contaminated (Alderton *et al*. 2014, Đorđević *et al*. 2017, Tasev *et al*. 2017, Đorđević *et al*. 2018), and even in the zones considered not to be affected by the former mining activities, similar concentrations were detected (Alderton *et al*. 2014).

Chemical compositions of the soil samples

Three samples of soil from locations separate from the mine dumps exhibit very high concentrations of arsenic from 81 to 1611 mg/kg As (median 1009 mg/kg) and antimony from 35 to 749 mg/kg Sb (median 605 mg/kg). As we assumed, sampling point 23, in the immediate vicinity of the flotation tailings, is particularly conspicuous with its high arsenic and antimony values (As > 1600 mg/kg and Sb > 749 mg/kg). Measured Mo and Tl values are also particularly high in that sample. All three soil samples have As and Sb contents which exceed proposed environmental quality limits (typically around 20 mg/kg for both elements), and even if a rather conservative threshold value of 50 mg/kg for both Sb and As is adopted, it is clear that many samples have contents of these elements which are above the 'intervention' values and are thus classed

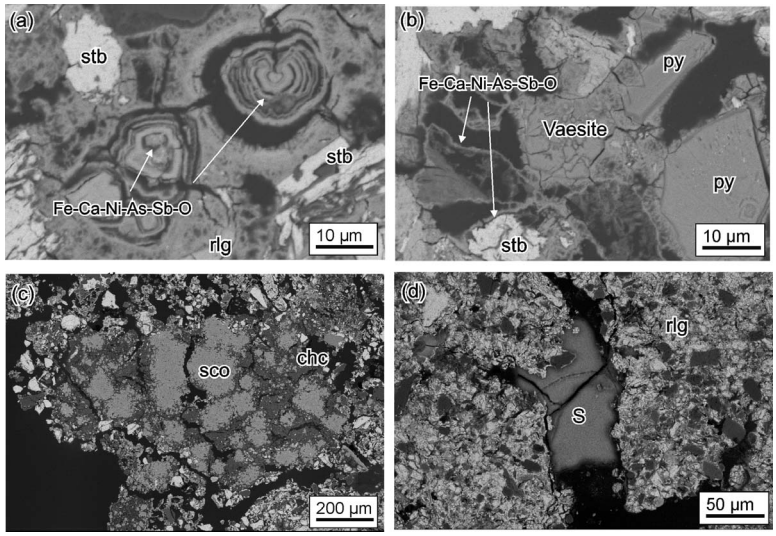

FIG. 4. Back-scattered electron images of tailings samples 6a and 6b. (a) Concentrically layered aggregates of an Fe-Ca-As-Sb-O(OH) phase in 6a. (b) Fractured vaesite (NiS_2) grains with pyrite (py) and stibnite (stb) crystals together with thin crusts of an Fe-Ca-As-Sb-O(OH) phase in 6a. (c) Overview showing massive and spherulitic scorodite (sco) and chalcedony (chc) with grains of quartz (dark) and realgar (bright) in 6b. (d) As-bearing sulfur (S) in realgar (rlg) in 6b.

as 'contaminated' and requiring remediation (Alderton *et al*. 2014, Tasev *et al*. 2017). In addition, these results are similar to those found for comparable abandoned mine sites elsewhere (Gal *et al*. 2007, Drahota & Filipi 2009, Alloway 2013). As mentioned earlier, there is a notable influence of the serpentinite on the samples, which is especially illustrated by high concentrations of Mg, Cr, and Ni in all three soil samples (MgO up to 18.32 wt.%, Cr up to 438 mg/kg, Ni up to 1119 mg/kg; Alderton *et al*. 2014). Statistical analysis performed on the soil compositions show that the highest correlation coefficients, as expected, occur for As–Sb (0.9781), As–Mo (0.9641), Sb–Mo (0.9982), Ni–Cr (0.9751), Pb–Cr (0.9302), and Pb–Ni (0.8258).

MINERALOGY OF THE TAILINGS

The cemented, porous, realgar-rich waste material was found to be a fine-grained mixture of the pre-weathering minerals (primary sulfides, mostly realgar) which were present in the tailings at the time of the deposition and their weathering products. According to the SEM studies of the polished samples, the grain size varies from <0.1 to (rarely) 250 µm. The average grain size is estimated to vary between 20 and 100 µm. In comparison to the most abundant pre-weathering minerals, such as realgar, stibnite, chromite, gypsum, and quartz, which could be easily distinguished using a binocular microscope, the weathering minerals were not easily recognized during preliminary investigations. This could be attributed to the small crystal size of the fine-grained material and the fact that these minerals formed *via* subrecent to recent weathering processes (the samples were collected from the surface and sub-surface of the tailings dump). Detailed descriptions of the studied samples and the list of identified minerals, including the methods used for their identification, are given in Table 2. Powder X-ray diffraction (PXRD) patterns with the results of their Rietveld analysis are presented in Figure S1 in the supplementary material. Selected SEM images are given in Figures 4 and 5, while selected Raman spectra are shown in Figure 6 and TEM images in Figure 7.

Primary minerals

The primary sulfide minerals realgar and stibnite are common in all analyzed samples. The same applies to quartz and gypsum (Table 2). In general, the main minerals in the tailings are realgar, gypsum, and quartz (Fig. 4), whereas stibnite is less abundant.

The two AsS polymorphs realgar and pararealgar represent the most abundant phases in all samples (average: ~55 wt.% per sample) and their presence was proven by all experimental methods. The SEM-EDX analyses of the polished sections showed that the majority of the tailings material consists of realgar fragments about 50–150 µm in size, which in samples 6a and 6c are invariably coated by very thin crusts of

TABLE 2. DETAILED DESCRIPTION OF THE STUDIED TAILINGS SAMPLES AND THE MOST ABUNDANT MINERALS ACCORDING TO PXRD, SEM-EDX, AND RAMAN-SPECTROSCOPIC ANALYSES

Sample	Color	Texture / hardness	Significant minerals	Ore minerals	Secondary minerals
6a	greyish-brown	from fine powder to grainy (grains up to 0.5 mm) / soft*	quartz[1–4], gypsum[1–4], vermiculite[1]	realgar[1–4], stibnite[1–4], chromite[2–4], pyrite[3,4], vaesite[4]	Fe–Ca–Ni–As–Sb–O phase[4], annabergite[1,4]
6b	light orange	from fine powder to grainy (grains up to 0.65 mm) / very soft**	quartz[1–4], gypsum[1–4]	realgar[1–4], stibnite[1–4], pararealgar[3], chromite[3,4], sphalerite[4]	scorodite[1,3,4], arsenolite[2], sulfur[1,3]
6c	yellowish-grey	from fine powder to fragments up to 1.5 cm / soft	quartz[1–4], gypsum[1–4], vermiculite[1]	realgar[1–4], stibnite[1–4], pyrite[4], gersdorffite[4]	scorodite[1], sulfur[1], Fe–Ca–Sb–As–O(OH) phase[3,4]
6d	yellow	from fine powder to fragments up to 2.5 cm / very soft	quartz[1–4], gypsum[1–4]	realgar[1–4], stibnite[1–3], pararealgar[1,3]	Fe–Ca–Sb–As–O(OH) phase[3,4], scorodite[1,3,4], sulfur[1,3], arsenolite[2]

* Could be crushed with a metal spoon; ** could be crushed with a fingernail.
[1] PXRD, [2] SXRD, [3] Raman, [4]SEM-EDX.

an As-Sb-Ca-Fe-(Ni)-oxide/hydroxide (Figs. 4 and 5). However, the size of the individual realgar grains can be less than 2 μm, but also up to 0.5 mm. The realgar is nearly always pure, with an As:S ratio near to 1, although some grains contain traces of Sb substituting for As. The color depends on the size; small grains show an orange color while larger grains appear red.

Stibnite occurs in the form of superficially corroded grains between 1 and 100 μm in size, partly embedded in either quartz or realgar. Stibnite is the second most abundant sulfide in the tailings. It is chemically either almost pure (samples 6a, 6b, and 6d) or it contains arsenic up to 4.8 at.% (sample 6c).

Rare relic Mg-rich chromite grains (up to ~20 μm) and, less commonly, magnesiochromite are always Al-bearing (7.8–14.4 at.%) and occur as anhedral, unaltered crystal fragments which are chemically homogeneous but show minor variations in the Cr:Al and Fe:Mg ratios among different grains. Chromite was found in all samples, except sample 6c.

Tiny euhedral to anhedral pyrite crystals (up to ~7 μm) are very rare and are found in samples 6a and 6c. They are always As-bearing (up to 2.2 at.% of As in 6a and up to 5 at.% in 6c). Pyrite from sample 6a contains trace amounts of Ni (up to 1.5 at.%). A few gersdorffite grains up to 5 μm are found in realgar (sample 6a) and quartz (6c). Vaesite (NiS_2) has been identified as inclusions in realgar (sample 6a) in the form of patchy aggregates (up to ~10 μm). One very small grain (~2 μm) of sphalerite embedded in quartz was found in sample 6b.

As representatives of the gangue minerals and country rocks, quartz (chalcedony), clay minerals (kaolinite–illite-vermiculite), muscovite, albite, fluorapatite, anatase/rutile, and epidote have been identified. Among these, quartz is very abundant (on average ~18.7 wt.% per sample), whereas the other minerals appear only as minor to trace components.

Secondary minerals

Secondary minerals in the tailings include gypsum, As-Sb-Ca-Fe-(Ni)-O(OH) roméite-group minerals, scorodite, arsenolite, pararealgar, native sulfur, annabergite, unidentified sulfo-arsenates, "limonite", kaatialaite(?), pickeringite, and alunogen. The last two phases were not detected in samples 6a–6d but were found only on the profile walls and during sampling in the dry period (Fig. 2e).

Gypsum, $CaSO_4 \cdot 2H_2O$, is the most abundant weathering phase. According to the Rietveld analyses, its amount ranges between 4.5 and 17.5 wt.%, depending on the sample. It is mostly present as white coatings formed by prismatic to needle-like single crystals up to 250 μm in length occurring on realgar.

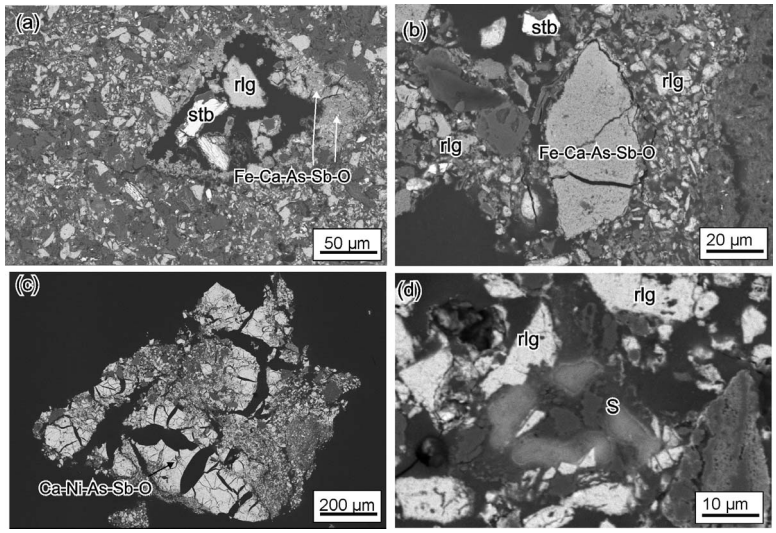

FIG. 5. Back-scattered electron images of samples 6c and 6d. (a) Recently grown Fe-Ca-As-Sb-O(OH) phase at the rims of the void in 6c. (b) 60 µm grain of an Fe-Ca-As-Sb-O(OH) phase in 6c. (c) Overview showing crack-like texture of the Ca-Ni-Sb-As-O(OH) phase, suggesting a prior gel state in 6d. (d) Sulfur (S) and realgar (rlg) in 6d.

Together with other sulfates (see below), it is the youngest mineral in this mineral assemblage. The EDX analyses reveal trace contents of As (AsO_4 replacing SO_4).

Pararealgar, AsS, represents the only secondary sulfide observed in the tailings and was detected in samples 6b and 6d (both having light orange color) by Raman spectroscopy and in sample 6d by PXRD. In sample 6d it is the dominant phase (~40 wt.%), whereas in sample 6b only minor amounts of pararealgar were found (Raman). It forms as a typical light-induced isochemical alteration product of realgar and is easily recognizable as an orange, thin, and fine-grained coating on any realgar lying on the tailings surface (as well as on weathered ore dumps; Kolitsch *et al*. 2018). Thus, the orange color of the surface of the tailings dump is due to the formation of pararealgar (Fig. 2a). The Raman spectrum of pararealgar is characterized by a pair of strong peaks at 221 and 232 cm^{-1} (supplementary material, Fig. S2) and a group of four distinguishable peaks centered at about 330 cm^{-1} (Trentelman & Stodulski 1996). Furthermore, the peak at 273 cm^{-1} appears only in pararealgar. In comparison to the Raman spectrum of realgar, the pararealgar spectrum has a greater number of bands of strong or medium intensity, reflecting the reduced molecular symmetry of pararealgar with respect to realgar.

Scorodite, $Fe^{3+}AsO_4 \cdot 2H_2O$, is the most widespread arsenate mineral in the tailings and was found in samples 6b and 6d. It usually occurs as a cement that fills the space among the mineral grains or in the form of massive or tiny spheroidal aggregates (Fig. 6a and b). In sample 6b it forms massive aggregates and in sample 6d it appears only sporadically in the form of elongate aggregates up to 40 µm in length that give the impression of being a former gel. The scorodite always contains traces of Sb (0.6–3.6 at.%), S (0.5–2.6 at.%), and Al (0.3–3.3 at.%), which is also reflected in the Raman spectra (supplementary material, Fig. S3) by the appearance of two Raman bands at 464 and 527 cm^{-1}, characteristic for the Sb^{5+}–O antisymmetric and symmetric stretching vibrations, respectively (Bahfenne & Frost 2010a). Other Raman bands (given in italics) correspond quite well with the Raman spectra reported for natural scorodites (Filippi *et al*. 2007, 2009, Kloprogge & Wood 2017) with major bands at ~180 (*181*), ~799 (*804*), and ~893 (*890*) cm^{-1}. The very strong bands at ~800 and ~900 cm^{-1} are assigned to As–O stretching in scorodite (Savage *et al*. 2005).

Rare native sulfur was identified in PXRD patterns and by SEM-EDX in all samples except 6a. Chemical analyses of the sulfur showed that it is always As-bearing (on average ~5 at.%). However, a few grains with 14 at.% arsenic on average were found in sample 6d.

Widespread, but volumetrically small, are thin crusts of As-Sb-Ca-Fe-(Ni)-O(OH) phases (with traces of S, Na, K, and Al) in which the As:Sb ratio varies from *ca*. 2:1 to 1:2.2 and Ca, Fe, and Ni contents are variable (Table 3). This generally inhomogeneous weathering product appears to be microcrystalline but

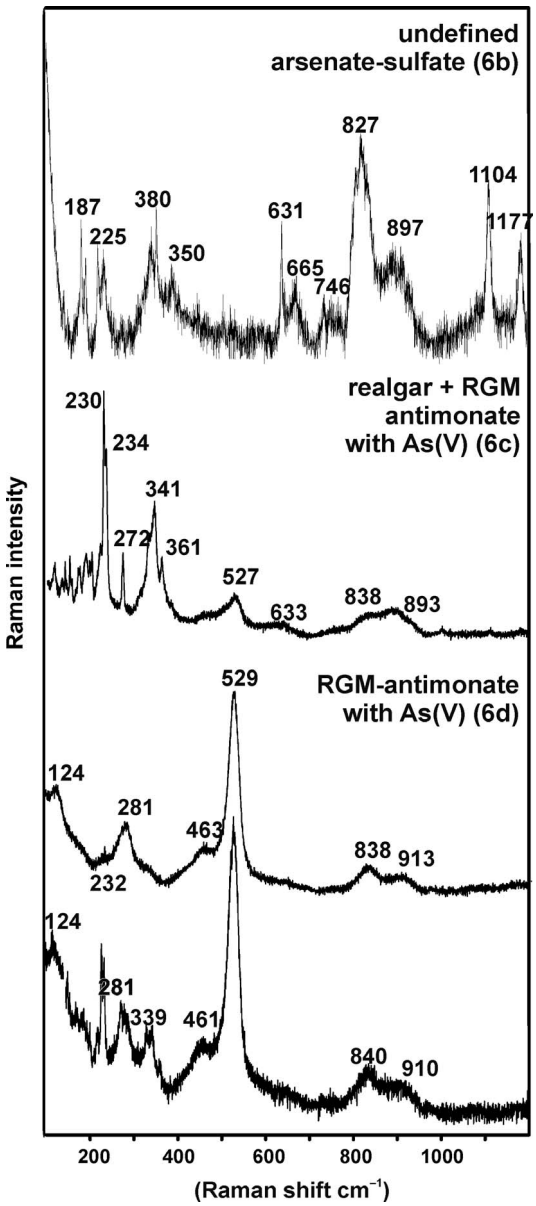

FIG. 6. Selected Raman spectra of the weathering phases (RGM = roméite-group mineral).

may in part be amorphous. According to the observed stoichiometry, crystalline forms probably belong, at least in part, to the roméite group of oxides, which itself belongs to the large pyrochlore supergroup of minerals (Atencio *et al*. 2010, Christy & Atencio 2013). The general formula of the pyrochlore supergroup is $^{[8]}A_{2-m}{}^{[6]}B_2X_{6-w}Y_{1-n}$ (A = Na, Ca, Ag, Mn, Sr, Ba, Fe^{2+}, Pb, Sn^{2+}, Sb^{3+}, Bi^{3+}, Y, REE, Sc, U, Th, vacancy, and H_2O; B = Ta, Nb, Ti, Sb^{5+}, W, V^{5+}, Sn^{4+}, Zr, Hf, Fe^{3+}, Mg, Al, and Si; X = O, OH, or F; and Y = $(OH)^-$, F^-, O^{2-}, vacancy, H_2O, or even large cations K^+, Rb^+, Cs^+) (Bosi *et al*. 2017). Sb(V) is the dominant cation at the B site in the roméite-group minerals (RGM). The latter have been identified as weathering products in smelting residues (Courtin-Nomade *et al*. 2012) and tailings (Klimko *et al*. 2011) resulting from Sb mining activities, and as the weathering products of tetrahedrite and tennantite (Borčinová Radková *et al*. 2017, Majzlan *et al*. 2018, Keim *et al*. 2018).

Besides forming very thin (<10 μm) encrustations (mostly As-dominant) around realgar and stibnite grains (Fig. 4), Sb-dominant variants of this oxide also form larger homogeneous grains up to 500 μm, characterized by broad dehydration cracks and suggesting original formation as a gel (Figs. 7 and 8). An As-rich As-Sb-Fe-Ca-O(OH) phase (Table 3) from sample 6c and an Sb-rich Sb-As-Fe-Ca-O(OH) phase from sample 6d were further analyzed by Raman spectroscopy (Fig. 6). The Raman spectra of both samples are most similar to the spectra of pyrochlore-supergroup antimonates. Bahfenne & Frost (2010a) analyzed Raman spectra of the mineral roméite group minerals, from three different localities. According to these authors, the intense Raman band around ~520 cm^{-1} is assigned to the Sb–O ν_1 symmetric stretching mode and the band around 466 cm^{-1} is assigned to the Sb–O ν_3 antisymmetric stretching mode. The Raman bands between 303 and 340 cm^{-1} are attributed to O–Sb–O bending modes. The Raman bands in these regions measured for samples 6c and 6d correspond quite well with the literature data and thus confirm the presence of Sb^{5+} in these phases. Additional weaker and broader bands in the region between 835 and 915 cm^{-1} (Fig. 6) correspond to the AsO_4 stretching vibrations (Bahfenne & Frost 2010b, Đorđević *et al*. 2016) and thus confirm the presence of As^{5+} in the structure. Recently, unusually As-rich and Cu-bearing roméite-group phases were described as weathering products of tetrahedrite–tennantite weathering (Borčinová Radková *et al*. 2017, Majzlan *et al*. 2018).

In order to characterize the As-Sb-Ca-(Fe)-(Ni)-O(OH) phases and their crystallinity in more detail, transmission electron microscopy (TEM) investigations were performed. Two phases were determined, one amorphous and one crystalline. The amorphous phase was found to be sensitive to electron beam irradiation and consists of As and S (former realgar). The crystalline phases – all appear to be oxides or hydroxides – are stable under electron beam irradiation. High-resolution (HR) TEM images consistently show the presence of Fe-Sb-As oxo-hydroxide nano-

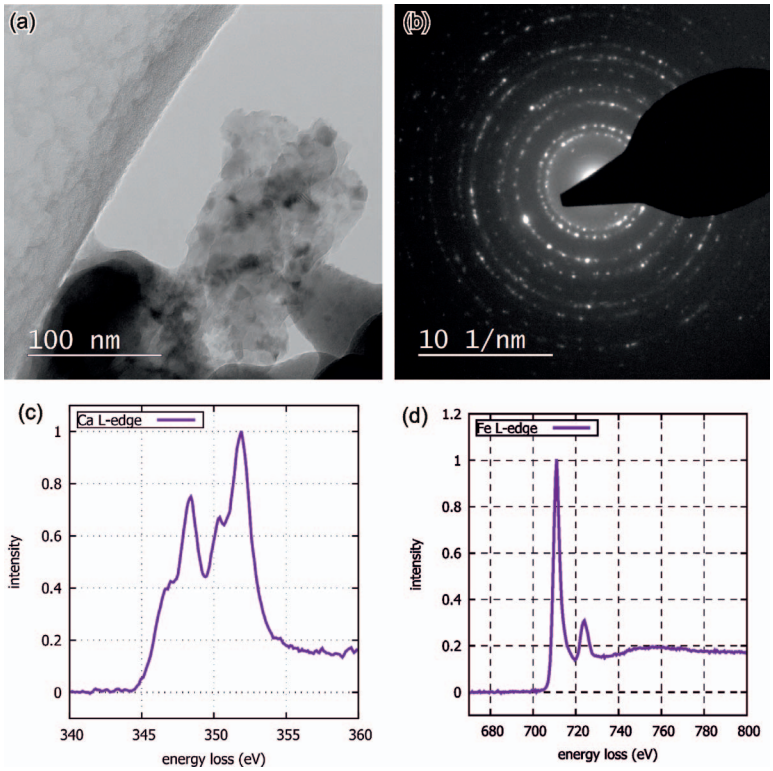

FIG 7. TEM images from tailings samples. (a) Typical particles of the roméite-group phase found in sample 6c. (b) Diffraction pattern showing the diffraction rings and a faint crystalline signature (diffraction spots). (c) Ca-*L* edge showing the ELNES (Energy Loss Near Edge Structure) spectrum of Ca^{2+}. (d) Fe-*L* edge showing the ELNES spectrum of Fe^{3+}.

TABLE 3. SEMI-QUANTITATIVE CHEMICAL ANALYSES (SEM-EDX) OF CHEMICALLY VARIABLE SECONDARY Fe-Ca-(Ni)-As-Sb-O(OH) PHASES FROM THE FLOTATION TAILINGS OF THE LOJANE MINE

Elements (at.%)*	Fe-Ca-Ni-As-Sb-O(OH)	Fe-Ca-As-Sb-O(OH)	Fe-Ca-As-Sb-O(OH)
# of spots	$n = 6$	$n = 3$	$n = 7$
Sample	6a	6c	6d
O	67 (65–68)	57 (54–61)	70 (68–71)
Na	0.5 (0.3–0.6)	0.45 (0.4–0.5)	—
Al	—	1.7 (0.7–3.3)	1.1 (0.3–2.1)
Si	0.7 (0.4–1.0)	1.6 (1.1–2.3)	1.0 (0.5–1.4)
K	—	—	0.7 (0.6–0.8)
Ca	5.3 (4.2–6.8)	1.9 (1.8–2.0)	3.7 (2.1–5.9)
Fe	6.0 (5.2–6.6)	9.0 (8.4–9.9)	4.9 (4.0–6.1)
Ni	2.1 (0.7–3.8)	—	—
As	10.83 (9.5–12.7)	16.9 (16.4–17.6)	15.4 (13.0–16.9)
Sb	7.2 (5.7–8.1)	11.0 (8.9–12.4)	21.8 (14.6–28.7)

* Normalized to 100%; estimated accuracy of cation values is better than 3–5% for major amounts and better than 20% for trace amounts.
n = number of spot analyses.

particles (Fig. 7a). There was no truly amorphous material detected among the Fe-Sb-As-oxides in the samples. Selected-area electron diffraction (Fig. 7b) was used to document the crystallinity of these nanoparticles. Due to the fact that the Ca-*K* edge partly overlaps with the Sb-*L* edge in the TEM-EDX analysis, EELS was used to identify Ca. Figure 7c presents the Ca-*L* edge at 356 eV energy loss, clearly showing the shape characteristic of Ca^{2+}. In the cases where iron was detected, its oxidation state was determined to be Fe^{3+} (Fig. 7d).

From the combination of SEM, TEM, and Raman measurements, it is likely that the analyzed thin crusts and aggregates are poorly crystalline to amorphous As-dominant RGM-like phases, darker grey in the SEM images (Fig. 5), and nano- to microcrystalline, Sb-dominant RMG, which are very light grey in the SEM and Raman images. The crystallographic position of arsenic in the RGM in our samples is not fully clear. Although As^{5+} may occupy the octahedrally coordinated *A* position in the roméite structure [a small number of natural and synthetic compounds containing AsO_6 octahedra are known: the mineral aerugite, $Ni_{8.5}As_3O_{16}$ (Fleet & Barbier 1989) and several alkali/silver-(H)-As-O compounds (Schwendtner & Kolitsch 2007 and references therein)], it strongly prefers a tetrahedral coordination. The distorted cubic (eight-coordinated) *B* position in RGM is too large for the As^{5+} cation. These crystal-chemical preferences explain why As is hosted mainly in the X-ray amorphous phases. However, EDX point analyses, both in our work and in Majzlan *et al*. (2018), clearly show that the roméite-type phase may incorporate considerable arsenic.

Arsenolite, As_2O_3, was identified in PXRD patterns (samples 6b and 6d). Besides being found in powdered bulk samples, arsenolite, together with the sulfates pickeringite, $MgAl_2(SO_4)_4{\cdot}22H_2O$, and alunogen, $Al_2(SO_4)_3(H_2O)_{12}{\cdot}5H_2O$, occurs as a minor phase on the surface of the profile walls. These minerals form on the surface of the tailings, probably over days and/or weeks. Both sulfate minerals were identified by Raman spectroscopy (supplementary materials, Fig. S3) and EDX analyses. The latter revealed that the pickeringite, which occurs as silky white fibrous aggregates, is chemically fairly homogeneous and Fe- and Ni^{2+}-bearing (Mg > Fe > Ni), the Fe most probably being in part trivalent; in addition, trace amounts of As were detected. Positions and relative intensities of the Raman bands of the measured pickeringite (in parentheses in italics) correspond quite well with major bands of the Fe-bearing pickeringite [~221 (*219*), ~315 (*314*), ~344 (*335*), ~424 (*428*), ~468 (*467*), ~530 (*531*), ~621 (*615*), ~976 (*975*), ~986 (*991*), ~995 (*996*), ~1071 (*1068*), ~1114 (*1115*), and ~1145 (*1145*) cm^{-1}] reported in the literature (Locke *et al*. 2007). The alunogen (tiny colorless platelets) is chemically pure. Positions of the alunogen Raman bands (in parentheses in italics) and their relative intensities show good agreement with major bands reported at ~156 (*156*), ~182 (*181*), ~191 (*191*), ~310 (*308*), ~342 (*344*), ~473 (*471*), ~528 (*527*), ~611 (*608*), ~992 (*992*), ~1086 (*1087*), and ~1127 (*1124*) cm^{-1} in the literature (Košek *et al*. 2018). Arsenolite was found in the form of very small (up to 15 μm) octahedral crystals dispersed on the surface of a gypsum crystal and as tiny, loose crystal aggregates. Raman bands of the measured arsenolite (in parentheses in italics) agree very well with major bands reported in the literature (Merrow *et al*. 2003): ~184 (*182*), ~268 (*266*), ~370 (*369*), and ~561 (*560*) cm^{-1}. Indistinct very few tiny, blocky grains of kaatialaite(?), or a chemically similar phase, were identified only by EDX.

Trace amounts of inhomogeneous iron oxyhydroxides were detected in samples 6b and 6d. The "limonite" aggregates may contain up to 3.2 at.% arsenic, 3.1 at.% antimony, and up to 1.5 at.% sulfur, among other very minor impurities, such as Al, Si, Ca, and Ti.

Sulfide Weathering and the Mobility of Contaminants

Behavior of arsenic

In contrast to the well-researched weathering of the Fe-bearing arsenic minerals, such as arsenopyrite and As-bearing pyrite (*e.g.*, Nesbitt *et al*. 1995, Corkhill & Vaughan 2009, Zhu *et al*. 2014), the natural weathering of Fe-free arsenic minerals, such as realgar and orpiment, is not well studied, despite their significant toxicity and their relative abundances in the environment.

In a recent study on the migration and transformation of arsenic in the realgar mining areas in China, Wu *et al*. (2017) reviewed the transformation principles and processes involving physical, chemical, and biological reactions in realgar. The results of their study showed that the migration processes lead to contamination of atmosphere, water, and soil in all realgar mining areas. However, Wu *et al*. (2017), like most other papers dealing with the weathering of realgar, does not answer the question of how As, Sb, and other toxic elements are hosted in the oxidation products. Instead, they focus mostly on the bulk chemical composition of the waste dumps and tailings but provide little information on the specific mineralogy and the important transformation pathways of the minerals. Only the recent mineralogical study of the As-bearing secondary minerals of the weathered oripiment-realgar tailings of the Shimen mine, China,

by Zhu *et al*. (2015) deals with the mineralogical behavior of arsenic during the natural weathering of realgar and orpiment. Zhu *et al*. (2015) identified the As-bearing secondary minerals in the weathered tailings and used these data to discuss the natural oxidation of orpiment and realgar and associated implications for the transformation and mobility of As.

Most information about the mobility and behavior of arsenic in neutral to alkaline conditions is derived from theoretical and laboratory-based experimental work (Lengke & Tempel 2003, 2005, Lengke *et al*. 2009 and references therein). From these studies we know that the oxidative dissolution rates of realgar increase with increasing pH values, dissolved oxygen concentrations, and temperature. For example, arsenic sulfide oxidation rates at near neutral to alkaline pH values are approximately three times to three orders of magnitude higher than those at pH ~2.

Quantum mechanical calculations of the realgar oxidation (Renock & Becker 2010) showed that at low pH (*i.e*., no co-adsorbing hydroxide) the paramagnetic ($^3O_2$) to diamagnetic ($^1O_2$) spin transition is the rate-limiting step of the oxidation. At high pH, the rate-limiting step is oxygen dissociation on the surface. The theoretically calculated oxidation rate ($\sim 1 \times 10^{-10}$ mol $m^{-2}s^{-1}$) is of the same order as empirically derived rates from experiments at $T = 298$ K, pH = 8, and similar dissolved oxygen concentrations.

Typically, the oxidative weathering and the light oxidation process, which proceed simultaneously, control transformation of the realgar-rich flotation tailings at Lojane. Naumov *et al*. (2007) found that on exposure to light, As in realgar can react with oxygen to generate As_2O_3, meaning that oxidation reactions are also involved in photo-induced conversions. Under natural conditions, photo-induced conversion would result in ~5% As_4S_4, 20% As_2O_3, and 75% para-realgar (Ballirano & Maras 2006). During this process, the As(II) in realgar directly transforms into As(III) and As(V). In the Lojane tailings, photo-induced conversion varies locally, depending on closeness to the dump surface, with up ~40% of the realgar transformed into pararealgar.

In iron-rich weathering environments, the arsenate anions are usually adsorbed on oxyhydroxide phases, resulting in reduced mobilization of arsenate into the environment. However, if the concentrations of bicarbonate and carbonate are high, As can be released from the surface of the iron oxyhydroxides back to the solution because of surface charge or may also act as a competitor for both As^{5+} and As^{3+} during sorption reactions (Lengke *et al*. 2009). In the Lojane flotation tailings, as well as in its waste dumps (Kolitsch *et al*. 2018), ferric iron oxyhydroxide phases are present only in insignificant quantities. Thus, the reduced mobilization of arsenate does not happen and only the precipitation of the dissolved arsenate as minor scorodite, annabergite, arsenolite, and As-bearing RGM phases precludes its further migration into the environment.

Similar to the Lojane tailings, the mineralization and general geology around the Shimen mine in China (Zhu *et al*. 2015) is Fe-poor and Ca-rich and the amount of As in its tailings is very high (33.97 wt.% As). At Shimen, the pH in the tailings is lower than at Lojane, and the As is generally immobilized in the form of acid Ca arsenates (weilite, pharmacolite), the acid Ca-Mg arsenate picropharmacolite, the Mg arsenate hörnesite, arsenolite, and As-bearing gypsum (SO_4^{2-}–$HAsO_4^{2-}$ substitution). The Ca arsenates have nearly perfect crystal morphologies and do not preserve any evidence of dissolution; they are highly soluble and as such cannot effectively immobilize As.

Behavior of antimony

The behavior of antimony during weathering of stibnite is quite different from that of arsenic. Co-precipitation and absorption of Sb(V) on amorphous Fe and Mn oxyhydroxides is rapid and also plays a significant role in controlling the mobility of Sb(V) in iron-rich weathering environments. However, if the concentration of Sb is high enough or if the weathering happens in an Fe-poor environment, such as at Lojane, secondary minerals of antimony will crystallize (Filella *et al*. 2009). Since Fe oxyhydroxides are rare at Lojane and Mn oxyhydroxides do not exist, Sb(III) prevails in the mine dumps in the form of Sb_2O_3 (valentinite and senarmontite), although strongly weathered stibnite ore has been partly transformed into stibiconite, a mixed Sb(III)–Sb(V) oxyhydroxide (Kolitsch *et al*. 2018). In the Lojane flotation tailings, antimony is mobilized in the form of the RGM phases. Minor amounts of antimony are also found in scorodite (up to 3.8 at.% of Sb) and in the few primary pyrite grains (up to 1.5 at.% of Sb). To date, comprehensive information about the solubility of RGM is missing.

Tripuhyite, a very important Sb-sink in Fe-As-Sb mine wastes, has not been reliably recognized at Lojane in the mining waste (Kolitsch *et al*. 2018) or in the flotation tailings, which is to be expected due to the Fe-poor environment.

At the Lojane deposit, ore minerals of both As and Sb formed simultaneously, which is typical for many similar geological environments (realgar/orpiment-stibnite mineralizations). Relative to Sb, under near-neutral and oxidizing conditions, As has a higher affinity for adsorption on Fe oxides such as goethite and ferrihydrite (Lalinská-Voleková *et al*. 2012). The weathering of the Fe-poor realgar concentrate in the

Lojane tailings, still containing significant amounts of stibnite (up to 13.5%), yields a mixture of nanocrystalline RMG antimonates and X-ray amorphous As-dominant RGM-like phases, in which both Sb and As, and partly Ni, are hosted. These widespread, but volumetrically minor, phases appear as very thin crusts around realgar and stibnite grains, but also as cement between these grains. Slightly Sb-bearing scorodite is also an important product of realgar and stibnite weathering. It occurs mostly as a cement that fills the space among the mineral grains and appears to be the result of rapid precipitation from oversaturated solutions at low temperatures. These conditions of formation might explain the apparent contradiction with the work of Kossoff *et al*. (2015), who synthesized scorodite in the presence of antimony at 140 °C and observed that the precipitated scorodite aggregates did not incorporate antimony; instead, tripuhyite ($FeSbO_4$) formed as an accompanying phase, the amount of which increased with increasing Sb in the synthesis. Kossoff *et al*. (2015) also observed no Sb in 36 natural samples of scorodite analyzed by EPMA. Since the Lojane scorodite formed at low temperature, seemingly often from a former gel, a metastable incorporation of minor Sb (as SbO_4^{3-}) in the structure appears possible. Alternatively, our samples might contain nanocrystalline tripuhyite undetectable by our analytical methods. However, scorodite controls As solubility only at pH less than 3 (DeSisto *et al*. 2011). Under circumneutral pH conditions, scorodite is metastable and breaks down to iron hydroxides and adsorbed/aqueous arsenate (Nordstrom *et al*. 2014).

Behavior of nickel and chromium

The mobilization of nickel during oxidation of Ni-bearing minerals occurring in the Lojane deposit, such as vaesite, Ni-bearing pyrite (up to 10 at.% of Ni), and gersdorffite, is reflected in the appearance of minor amounts of secondary annabergite, $Ni_3(AsO_4)_2{\cdot}8H_2O$, and secondary Ni-bearing RGM (with up to 3.8 at.% of Ni). Chemical analyses of the tailings samples show the highest Ni content of 5640 mg/kg in sample 6a (in which both vaesite and gersdorffite were detected) and the smallest content of 103 mg/kg of Ni in sample 6d. Geochemical studies of soils and sediments in the immediate vicinity of the flotation tailings at the Lojane deposit showed maximum Ni content of 1119 mg/kg (Alderton *et al*. 2014).

Present studies of the flotation tailings material (this work) and the mine dumps (Kolitsch *et al*. 2018) at Lojane indicate only negligible mobilization of Cr by weathering processes. Grains of chromite and magnesiochromite show neither rims of any secondary Cr minerals formed around these grains, nor Cr as an impurity element in other secondary phases. These observations are in agreement with literature data on weathered Cr deposits (Garnier *et al*. 2008) and are explained by the extreme stability of the chromite and magnesiochromite at low temperatures. Chemical analyses show that the Cr content in our tailings samples varies between 632 and 796 mg/kg. In soils and sediments in the immediate vicinity of the flotation tailings, a Cr content of up to 595 mg/kg was measured, with a median value of 285 mg/kg (Alderton *et al*. 2014, Tasev *et al*. 2017).

The influence of microbial activity was not considered in this study, but it is well known that microbes not only are able to oxidize the As(II) in realgar to As(III), and to transform the As(III), which is produced by photochemical oxidation reactions, into As(V) (*e.g.*, Paikaray 2015 and references cited therein), but that they can oxidize S at the same time (Morin *et al*. 2003). For example, some sulfate respiratory bacteria and S-oxidizing bacteria can change the chemical speciation and valence state of As in realgar by affecting the form of elemental S. By utilizing As and S as their growth substrate, S-oxidizing bacteria can change the form and valence of As by combining with chemical reactions during growth (Fisher *et al*. 2008). On the other hand, in As- and Sb-containing tailings and smelting residues, Sb was observed to negatively affect several types of bacteria (Courtin-Nomade *et al*. 2012).

Conclusions

The unique realgar concentrate in the flotation tailings of the Lojane mine was studied from a mineralogical point of view. The fine-grained concentrate has been oxidizing for at least 40 years. Chemical and mineralogical analyses of the tailings dump show that samples are mostly composed of realgar, quartz, and gypsum, followed by stibnite, pararealgar, sulfur, scorodite, and compositionally variable Fe-As-Sb-Ca-(Ni)-O(OH) phases belonging to the roméite group. Relic pyrite and vaesite, as well as the weathering products arsenolite, annabergite, "limonite", pickeringite, and alunogen, are present in minor quantities. Secondary phases mostly form the cement among the fine-grained realgar/pararealgar, stibnite, and quartz.

The weathering of primary sulfides in the flotation tailings at Lojane over the past 40 years proceeded under mostly oxidizing, acidic, and temporarily wet conditions. Highly acidic conditions on the surface of the concentrate body imply dissolution of arsenolite and scorodite, thus causing contamination of the environment and high mobility of arsenic. This assumption is supported by high arsenic soil and groundwater

concentrations determined in close proximity to the concentrate body (Alderton *et al*. 2014).

The oxidation and decomposition of the realgar-rich flotation tailings at Lojane resulted in the formation of various secondary phases whose stabilities affect the release or retention of elements in the near-surface oxidizing and wet environment. The oxidation of primary sulfides releases significant amounts of potentially toxic elements, mostly Sb, As, Ni, and Cr, which are hosted differently in these oxidation products. The concentration of arsenic is the highest in arsenolite, scorodite, and amorphous to poorly crystalline roméite-type phases. However, minor amounts of arsenic are also present in gypsum, sulfur, and pickeringite, which is explained by the abundance of realgar in the tailings and the consequently As^{5+}-rich weathering solutions percolating through the porous tailings material. This observation shows that migration of As into the environment may also depend on the role of secondary sulfates in the tailings.

The primary oxidation source of antimony is stibnite; during weathering, Sb mostly enters nanocrystalline Fe^{3+}-rich roméite-group phases. The situation at Lojane is similar to that at a historic antimony mine in New Zealand where negligible attenuation of the metalloids Sb and As (from arsenopyrite) occurred *via* adsorption outside the adit, as iron oxyhydroxide is rare at the New Zealand mine site (Wilson *et al*. 2004). At Lojane, antimony is less mobile compared to As; this agrees well with literature data (*e.g*., Fawcett & Jamieson 2011, Fawcett *et al*. 2015).

Considering the only minor presence of pyrite in the Lojane mineralization, the pH-buffering geological environment (*e.g*., limestone, dolostone, marble, silicified serpentinite), and the carbonate gangue (*e.g*., dolomite, calcite) that produce neutral to slightly alkaline local waters, it is likely that As and partly Sb stay in solution and can be transported over greater distances. Furthermore, fine-grained and thus very light tailings material is also subject to continued physical transport *via* wind, threatening a wider area. The remediation of this environmental hot spot remains unresolved due to local socio-political tensions.

Acknowledgments

The financial support of the Austrian Science Fund (FWF) (P 30900-N28) and the Federal Ministry of Science, Research and Economy, Scientific & Technological Cooperation between Macedonia and Austria 2016-2018 (Grant MK 05/2016) is gratefully acknowledged. We thank Dr. Karolina Schwendtner for assisting during the Rietveld analysis. Reviews by Prof. Dr. Dave Craw and an anonymous reviewer were helpful in improving the manuscript.

References

Alderton, D., Serafimovski, T., Burns, L., & Tasev, G. (2014) Distribution and mobility of arsenic and antimony at mine sites in FYR Macedonia. *Carpathian Journal of Earth and Environmental Sciences* **9**, 43–56.

Alexander, B. (2008) *Trace element analysis in geological material using low resolution inductively coupled plasma mass spectrometry (ICPMS)*. Technical Report 18, Jacobs University Bremen, School of Engineering and Science, Bremen.

Alloway, B.J. (2013) *Heavy metals in soils: Trace metals and metalloids in soils and their bioavailability, 3rd Edition*. Springer Science + Business Media, Dordrecht, Netherlands, 614 pp.

Antonović, A. (1965) Geology, tectonic structure and genesis of the arsenic-antimony ore deposits in the Lojane and Nikuštak district (Skopska Crna Gora Mts). Geological Institute, Skopje, Special Issue 1, 77 pp. (in Macedonian).

Ashley, P.M., Craw, D., Graham, B.P., & Chappell, D.A. (2003) Environmental mobility of antimony around mesothermal stibnite deposits, New South Wales, Australia and southern New Zealand. *Journal of Geochemical Exploration* **77**, 1–14.

Atencio, D., Andrade, M.B., Christy, A.G., Gieré, R., & Kartashov, P.M. (2010) The pyrochlore supergroup of minerals: nomenclature. *Canadian Mineralogist* **48**, 673–698.

Augé, T., Morin, G., Bailly, L., & Serafimovsky, T. (2017) Platinum-group minerals and their host chromitites in Macedonian ophiolites. *European Journal of Mineralogy* **29**, 585–596.

Bahfenne, S. & Frost, R.L. (2010a) Raman spectroscopic study of the antimonate mineral roméite. *Spectrochimica Acta Part A: Molecular and Biomolecular Spectroscopy* **A75**, 637–639.

Bahfenne, S. & Frost, R.L. (2010b) A review of the vibrational spectroscopic studies of arsenite, antimonite, and antimonate minerals. *Applied Spectroscopy Reviews* **45**, 101–129.

Ballirano, P. & Maras, A. (2006) *In-situ* X-ray transmission powder diffraction study of the kinetics of the light induced alteration of realgar (α-As_4S_4). *European Journal Mineralogy* **18**, 589–599.

Borčinová Radková, A., Jamieson, H., Lalinská-Voleková, B., Majzlan, J., Števko, M., & Chovan, M. (2017) Mineralogical controls on antimony and arsenic mobility during tetrahedrite-tennantite weathering at historic mine sites Špania Dolina-Piesky and Ľubietová-Svätodušná, Slovakia. *American Mineralogist* **102**, 1091–1100.

Bosi, F., Christy, A.G., & Hålenius, U. (2017) Crystal-chemical aspects of the roméite group, $A_2Sb_2O_6Y$, of the pyrochlore supergroup. *Mineralogical Magazine* **81**, 1287–1302.

Bruker (2017) *TOPAS*, Version 6. Bruker AXS, Karlsruhe, Germany.

Burton, E.D., Hockmann, K., Karimian, N., & Johnston, S.G. (2019) Antimony mobility in reducing environments: The effect of microbial iron(III)-reduction and associated secondary mineralization. *Geochimica et Cosmochimica Acta* **245**, 278–289.

Christy, A.G. & Atencio, D. (2013) Clarification of status of species in the pyrochlore supergroup. *Mineralogical Magazine* **77**, 13–20.

Corkhill, C.L. & Vaughan, D.J. (2009) Arsenopyrite oxidation – A review. *Applied Geochemistry* **24**, 2342–2361.

Courtin-Nomade, A., Rakotoarisoa, O., Bril, H., Grybos, M., Forestier, L., Foucher, F., & Kunz, M. (2012) Weathering of Sb-rich mining and smelting residues: Insight in solid speciation and soil bacteria toxicity. *Chemie der Erde - Geochemistry* **72**, 29–39.

DeSisto, S.L., Jamieson, H.E., & Parsons, M.B. (2011) Influence of hardpan layers on arsenic mobility in historical gold mine tailings. *Applied Geochemistry* **26**, 2004–2018.

Divljan, S. (1957) Results of the Lojane mine effusive rocks analyses. *Bulletin du Muséum d'histoire naturelle de Belgrade: Série A* **12**, 111–149 (in Serbian).

Đorđević, T., Kolitsch, U., & Nasdala, L. (2016) A single-crystal X-ray and Raman spectral study of hydrothermally synthesized arsenates and vanadates of descloizite and adelite structure-types. *American Mineralogist* **101**, 1135–1149.

Đorđević, T., Kolitsch, U., Tasev, G., Serafimovski, T., & Boev, B. (2017) Anomalous As-enrichment in gersdorffite in a realgar-rich environment: Lojane, Macedonia. *Mitteilungen der Österreichischen Mineralogischen Gesellschaft* **163**, 38 (abstract).

Đorđević, T., Kolitsch, U., Tasev, G., Serafimovski, T., & Boev, B. (2018) First insights into the mineralogy of the tailings dump of the Lojane Sb-As(-Cr) deposit, FYR of Macedonia. EGU General Assembly 2018, Vienna, Austria, *Geophysical Research Abstracts* **20**, EGU2018-14914.

Drahota, P. & Filippi, M. (2009) Secondary arsenic minerals in the environment: A review. *Environment International* **35**, 1243–1255.

Dulski, P. (2001) Reference materials for geochemical studies: New analytical data by ICP-MS and critical discussion of reference values. *Geostandards Newsletter* **25**, 87–125.

Fawcett, S.E. & Jamieson, H.E. (2011) The distinction between ore processing and post-depositional transformation on the speciation of arsenic and antimony in mine waste and sediment. *Chemical Geology* **283**, 109–118.

Fawcett, S.E., Jamieson, H.E., Nordstrom, D.K., & McCleskey, R.B. (2015) Arsenic and antimony geochemistry of mine wastes, associated waters and sediments at the Giant Mine, Yellowknife, Northwest Territories, Canada. *Applied Geochemistry* **62**, 3–17.

Filella, M., Williams, P.A., & Belzile, N. (2009) Antimony in the environment: knowns and unknowns. *Environmental Chemistry* **6**, 95–105.

Filippi, M., Doušová, B., & Machovič, V. (2007) Mineralogical speciation of arsenic in soils above the Mokrsko-west gold deposit, Czech Republic. *Geoderma* **139**, 154–170.

Filippi, M., Machovič, V., Drahota, P., & Böhmová, V. (2009) Raman microspectroscopy as a valuable additional method to X-ray diffraction and electron microscope/microprobe analysis in the study of iron arsenates in environmental samples. *Applied Spectroscopy* **63**, 621–626.

Fisher, J.C., Wallschlager, D., Planer-Friedrich, B., & Hollibaugh, J.T. (2008) A new role for sulfur in arsenic cycling. *Environmental Science and Technology* **42**, 81–85.

Fleet, M.E. & Barbier, J. (1989) Structure of aerugite ($Ni_{8.5}As_3O_{16}$) and interrelated arsenate and germanate structural series. *Acta Crystallographica* **B45**, 201–205.

Flynn, H.C., Meharg, A.A., Bowyer, P.K., & Paton, G.I. (2003) Antimony bioavailability in mine soils. *Environmental Pollution* **124**, 93–100.

Gal, J., Hursthouse, A., & Cuthbert, S. (2007) Bioavailability of arsenic and antimony in soils from an abandoned mining area, Glendinning (SW Scotland). *Journal of Environmental Science and Health* **A42**, 1263–1274.

Garnier, J., Quantin, C., Guimarães, E., & Becquer, T. (2008) Can chromite weathering be a source of Cr in soils?. *Mineralogical Magazine* **72**, 49–53.

Grafenauer, S. (1977) Genesis of chromite in Yugoslavian peridotite. *In* Time- and Strata-Bound Ore Deposits (D.D. Klemm & H.-J. Schneider, eds.). Springer, Verlag – Berlin – Heidelburg (327–351).

Gripp, K. (1922) Beiträge zur Geologie von Mazedonien. Universität Hamburg, *Abhandlungen auf dem Gebiet der Auslandkunde, Band 7 — Reihe C: (Naturwissenschaften) Band* **3**, 61 pp.

Hiessleitner, G. (1931) Geologie mazedonischer Chromeisenlagerstätten. *Berg- und Hüttenmännisches Jahrbuch der Montanistischen Hochschule in Leoben* **79**, 47–57 (in German).

Hiessleitner, G. (1934) Einbruch von Granit und Andesit in Chromerze führenden Serpentin von Lojane, NNW

Kumanovo in Südserbien. *Zeitschrift für Praktische Geologie* **42**, 81–88 (in German).

Hiessleitner, G. (1951) Serpentin- und Chromerz-Geologie der Balkanhalbinsel und eines Teiles von Kleinasien. *Jahrbuch der Geologischen Bundesanstalt Sonderband* **1**, 1–255 (in German).

Hudson-Edwards, K.A. (2016) Tackling mine wastes. *Science* **352**, 288–290.

Janković, S.R. (1960) Allgemeine Charakteristika der Antimonerzlagerstätten Jugoslawiens. *Neues Jahrbuch für Mineralogie Abhandlungen* **94**, 506–538 (in German).

Janković, S.R. (1989) Sb-As-Tl mineral associations in the Mediterranean region. *International Geology Review* **31**, 262–273.

Japan International Cooperation Agency (JICA), Ministry Of Agriculture, Forestry And Water Economy (MAFWE), The Former Yugoslav Republic Of Macedonia (2008) *The study on capacity development for soil contamination management related to mining in the Former Yugoslav Republic of Macedonia*. Final Report, Vol. II, Main Report, March 2008, Mitsubishi Materials Natural Resources Development Corporation, 159 pp.

Keim, M., Staude, S., Marquardt, K., Bachmann, K., Opitz, J., & Markl, G. (2018) Weathering of Bi-bearing tennantite. *Chemical Geology* **499**, 1–25.

Klimko, T., Lalinská, B., Majzlan, J., Chovan, M., Kučerová, G., & Paul, C. (2011) Chemical composition of weathering products in neutral and acidic mine tailings from stibnite exploitation in Slovakia. *Journal of Geosciences* **6**, 327–340.

Kloprogge, T. & Wood, B.J. (2017) X-ray photoelectron spectroscopic and Raman microscopic investigation of the variscite group minerals: Variscite, strengite, scorodite and mansfieldite. *Spectrochimica Acta Part A: Molecular and Biomolecular Spectroscopy* **185**, 163–172.

Kolitsch, U., Đorđević, T., Tasev, G., Serafimovski, T., Boev, I., & Boev, B. (2018) Supergene mineralogy of the Lojane Sb-As-Cr deposit, Republic of Macedonia: Tracing the mobilisation of toxic metals. *Geologica Macedonica* **32**, 95–117.

Košek, F., Culka, A., Žáček, V., Laufek, F., Škoda, R., & Jehlička, J. (2018) Native alunogen: A Raman spectroscopic study of a well-described specimen. *Journal of Molecular Structure* **1157**, 191–200.

Kossoff, D., Welch, M.D., & Hudson-Edwards, K.A. (2015) Scorodite precipitation in the presence of antimony. *Chemical Geology* **406**, 1–9.

Lalinská-Voleková, B., Majzlan, J., Klimko, T., Chovan, M., Kucerova, G., Michňová, J., Hovorič, R., Goettlicher, J., & Steininger, R. (2012) Mineralogy of weathering products of Fe-As-Sb mine wastes and soils at several Sb deposits in Slovakia. *Canadian Mineralogist* **50**. 1207–1226.

Lengke, M.F. & Tempel, R.N. (2003) Natural realgar and amorphous AsS oxidation kinetics. *Geochimica and Cosmochimica Acta* **67**, 859–871.

Lengke, M.F. & Tempel, R.N. (2005) Geochemical modeling of arsenic sulfide oxidation kinetics in a mining environment. *Geochimica and Cosmochimica Acta* **69**, 341–356.

Lengke, M.F., Sanpawanitchakit, C., & Tempel, R.N. (2009) The oxidation and dissolution of arsenic-bearing sulfides. *Canadian Mineralogist* **47**, 593–613.

Locke, A.J., Martens, W.N., & Frost, R.L. (2007) Natural halotrichites – an EDX and Raman spectroscopic study. *Journal of Raman Spectroscopy* **38**, 1429–1435.

Majzlan, J., Lalinská, B., Chovan, M., Jurkovič, L., Milovská, S., & Göttlicher, J. (2007) The formation, structure, and ageing of As-rich hydrous ferric oxide at the abandoned Sb deposit Pezinok (Slovakia). *Geochimica et Cosmochimica Acta* **71**, 4206–4220.

Majzlan, J., Lalinská, B., Chovan, M., Bläß, U., Brecht, B., Göttlicher, J., Steininger, R., Hug, K., Ziegler, S., & Gescher, J. (2011) A mineralogical, geochemical, and microbiological assessment of the antimony- and arsenic-rich neutral mine drainage tailings near Pezinok, Slovakia. *American Mineralogist* **96**, 1–13.

Majzlan, J., Drahota, P., & Filippi, M. (2014) Paragenesis and crystal chemistry of arsenic minerals. *Reviews in Mineralogy and Geochemistry* **79**, 17–184.

Majzlan, J., Kiefer, S., Herrmann, J., Števko, M., Sejkora, J., Chovan, M., Lánczos, T., Lazarov, M., Gerdes, A., Langenhorst, F., Borčinová Radková, A., Jamieson, H., & Milovský, R. (2018) Synergies in elemental mobility during weathering of tetrahedrite [$(Cu,Fe,Zn)_{12}Sb,As)_4S_{13}$]: Field observations, electron microscopy, isotopes of Cu, C, O, radiometric dating, and water geochemistry. *Chemical Geology* **488**, 1–20.

Merrow, C.N., Kirkby, S.J., Jensen, J.O., Zeroka, D., & Banerjee, A. (2003) Raman spectroscopy of arsenolite: Crystalline cubic As_4O_6. *Journal of Solid State Chemistry* **173**, 54–58.

Mohan, D. & Pittman, C.U., Jr. (2007) Arsenic removal from water/wastewater using adsorbents - A critical review. *Journal of Hazardous Materials* **142**, 1–53.

Morin, G., Juillot, F., Casiot, C., Bruneel, O., Personné, J.-C., Elbaz-Poulichet, F., Leblanc, M., Ildefonse, P., & Calas, G. (2003) Bacterial formation of tooeleite and mixed As^{3+}/(V)-Fe^{3+} gels in the Carnoules acid mine drainage, France. A XANES, XRD, and SEM study. *Environmental Sciences and Technology* **37**, 1705–1712.

Naumov, P., Makreski, P., & Jovanovski, G. (2007) Direct atomic scale observation of linkage isomerization of As_4S_4 clusters during the photoinduced transition of realgar to pararealgar. *Inorganic Chemistry* **46**, 10624–10631.

Nesbitt, H.W., Muir, I.J., & Prarr, A.R. (1995) Oxidation of arsenopyrite by air and air-saturated, distilled water, and implications for mechanism of oxidation. *Geochimica et Cosmochimica Acta* **59**, 1773–1786.

Nordstrom, K.D., Majzlan, J., & Königsberger, E. (2014) Thermodynamic properties for arsenic minerals and aqueous species. *Reviews in Mineralogy and Geochemistry* **79**, 217–255.

Paikaray, S. (2015) Arsenic geochemistry of acid mine drainage. *Mine Water and the Environment* **34**, 181–196.

Radusinović, D.R. (1956) *The mineral composition and structural features of the sulfide deposit of Lojane*. Internal Report, Establ. Nuclear Raw Materials, Beograd, Yugoslavia (in Serbian).

Radusinović, D.R. (1966) Greigite from the Lojane chromium deposit, Macedonia. *American Mineralogist* **51**, 209–215.

Renock, D. & Becker, U. (2010) A first principles study of the oxidation energetics and kinetics of realgar. *Geochimica et Cosmochimica Acta* **74**, 4266–4284.

Roper, A.J., Williams, P.A., & Filella, M. (2012) Secondary antimony minerals: Phases that control the dispersion of antimony in the supergene zone. *Chemie der Erde* **72**, Supplement 4, 9–14.

Savage, K.S., Bird, D.K., & O'Day, P.A. (2005) Arsenic speciation in synthetic jarosite. *Chemical Geology* **215**, 473–498.

Schumacher, F. (1954) The ore deposits of Yugoslavia and the development of its mining industry. *Economic Geology* **49**, 451–492.

Schwendtner, K. & Kolitsch, U. (2007) Octahedral As in M^{+} arsenates - architecture and seven new members. *Acta Crystallographica* **B63**, 205–215.

Serafimovski, T. (1993) Structural-metallogenic features of the Lece-Chalkidiki zone: Types of mineral deposit and distribution. Faculty of Mining, Štip, Special Issue No. 2, 325 pp.

Tasev, G., Serafimovski, T., Đorđević, T., & Boev, B. (2017) Soil and groundwater contamination around the Lojane As-Sb mine, Republic of Macedonia. 17th International Multidisciplinary Scientific GeoConference SGEM 2017, 29 June–5 July, Albena, Bulgaria, Conference Proceedings **17**, 809–817.

Trentelman, K. & Stodulski, L. (1996) Characterization of pararealgar and other light-induced transformation products from realgar by Raman microspectroscopy. *Analytical Chemistry* **68**, 1755–1761.

Tućan, F. (1936) Syenite, Granite und Dazite von Lojane in der Skopska Crna Gora. *Papers of Yugoslavian academy of sciences and arts* **254/79**, 29–110 (in German).

United Nations Environment Progamme (UNEP) (2000) *Post-Conflict Environmental Assessment – FYR of Macedonia*. UNEP, Geneva, Switzerland, 88 pp.

United States Environmental Protection Agency (USEPA) (2009) National primary drinking water regulations. EPA 816-F-09-004, Washington, 7 pp.

Williams, S. & Marstijepović, S. (2010) Western Balkans environmental program: Case studies on remediation of environmental hot spots in the western Balkans. UNDP Montenegro, 176 pp.

Wilson, N.J., Craw, D., & Hunter, K. (2004) Contributions of discharges from a historic antimony mine to metalloid content of river waters, Marlborough, New Zealand. *Journal of Geochemical Exploration* **84**, 127–139.

Wu, Y., Zhou, X.-Y., Lei, M., Yang, J., Ma, J., Qiao, P.-W., & Chen, T.-B. (2017) Migration and transformation of arsenic: Contamination control and remediation in realgar mining areas. *Applied Geochemistry* **77**, 44–51.

Zhu, T.T., Lu, X.C., Liu, H., Li, J., Zhu, X.Y., Lu, J.J., & Wang, R.C. (2014) Quantitative X-ray photoelectron spectroscopy-based depth profiling of bioleached arsenopyrite surface by Acidithiobacillus ferrooxidans. *Geochimica et Cosmochimica Acta* **127**, 120–139

Zhu, X., Wang, R., Lu, X., Liu, H., Li, J., Ouyang, B., & Lu, J. (2015) Secondary minerals of weathered orpiment-realgar-bearing tailings in Shimen carbonate-type realgar mine, Changde, Central China. *Mineralogy and Petrology* **109**, 1–15.

Received December 11, 2018. Revised manuscript accepted March 20, 2019.